Nuclear Inst. and Methods in Physics Research, A 947 (2019) 162712

Contents lists available at ScienceDirect

Nuclear Inst. and Methods in Physics Research, A

journal homepage: www.elsevier.com/locate/nima

Development of a high-performance W-band duplexer for plasma diagnosis using a single band with dual circular polarization

José R. Montejo-Garai [a,*], Carlos A. Leal-Sevillano [b], Jorge A. Ruiz-Cruz [c], Jesús M. Rebollar [a]

[a] Grupo de Electromagnetismo Aplicado, Information Processing and Telecommunications Center, Universidad Politécnica de Madrid, 28040 Madrid, Spain
[b] SENER, Ctra. Campo Real, km 2,100, 28500 Arganda del Rey, Madrid, Spain
[c] Escuela Politécnica Superior, Universidad Autónoma de Madrid, 28049 Madrid, Spain

ARTICLE INFO

Keywords:
Waveguide duplexer
Orthomode transducer
Circular polarization
Axial ratio
Return loss
Isolation and plasma diagnosis

ABSTRACT

This work presents the design and experimental validation of a high performance, compact, waveguide duplexer operating from 91.5 to 96.5 GHz for its integration in diverse W-band microwave equipment as in plasma diagnosis applications. It uses a single frequency band, with two signals discriminated by different orthogonal circular polarization, which is generated by means of a septum orthomode transducer (OMT) polarizer. Moreover, this component is optimized loaded with the horn antenna for improving the overall system performance. It is explained how these two components are integrated into a very compact duplexer, designed using efficient numerical algorithms. The manufacturing process by mean of high precision milling, and including electrical discharge machining (EDM) has led to excellent performances. The measured return loss level and isolation are higher than 30 dB, and the insertion loss level is below 0.3 dB. Finally, the key parameter in this device, which reflects the symmetry in the manufacturing process, i.e., the axial ratio, is lower than 0.6 dB for both polarizations, an excellent result showing the potential of the presented design.

1. Introduction

Dual polarized antenna systems are extensively used for satellite communications systems [1,2], radio astronomy [3–5] as well as for radars for different applications such as weather, air traffic control or imaging [6–9]. In these systems, different schemes are used with respect to the selection of frequency bands and polarization for transmission and reception [9]. With the progressive development of applications at new frequency bands [10], the hardware of the transceivers has become especially challenging, since classical schemes working at lower frequency bands cannot be directly translated to this new frequency bands in many cases. This has opened new areas of research for improving the performance of components and systems in particle accelerators, molecular spectroscopy or plasma diagnosis [11–13], leading to new system configurations for the microwave equipment at these high frequency bands, as it is done in this paper.

The circular polarization has been used for the characterization of anisotropic plasmas at least since 1960s [14]. More recently, different works have been published to highlight the interest of the circular polarization in the Thomson scattering technique for plasma characterization [15–17]. In this work, a circular polarization duplexer is introduced, whose basic scheme is shown in Fig. 1. It is a suitable scheme to isolate transmitter and receiver signals that operate simultaneously in the same frequency band, but with orthogonal circular polarized signals, while maintaining low losses between the generator and the antenna. Its use is an option when ferrite based circulators become not suitable [8,18], as it is the case of the targeted W-band considered in this work. Assuming normal incidence of a circular polarized plane wave on an isotropic target, considering in a first approach an isotropic medium, the reflected wave will be in the opposite orthogonal circular polarization. For example, if the incident field has for reference left-hand circular polarization (C−), as a result of the reflection, its direction of propagation reverses while maintaining the original sense of electric field rotation, resulting in a backscattered field with right-hand circular polarization (C+). Therefore, the duplexer can be implemented by transmitting in one circular polarization and receiving in the orthogonal one, separating both signals with the same frequency at different physical ports, as illustrated in Fig. 1. For an actual plasma whose reflection is a general elliptic polarized wave, the decomposition in two orthogonal circular waves of Fig. 1 is done, and the detector would capture the C+ component. The power source of the transmitter would be isolated by the block between the source and transmitter port of the duplexer, as in typical microwave equipment, which can be implemented in diverse ways, such as using hybrid couplers and dissipative loads.

Waveguide technology is the most suitable for high-frequency systems requiring high power capability, low insertion loss and rigid

* Corresponding author.
E-mail address: jr@etc.upm.es (J.R. Montejo-Garai).

https://doi.org/10.1016/j.nima.2019.162712
Received 9 May 2019; Received in revised form 30 July 2019; Accepted 5 September 2019
Available online 12 September 2019
0168-9002/

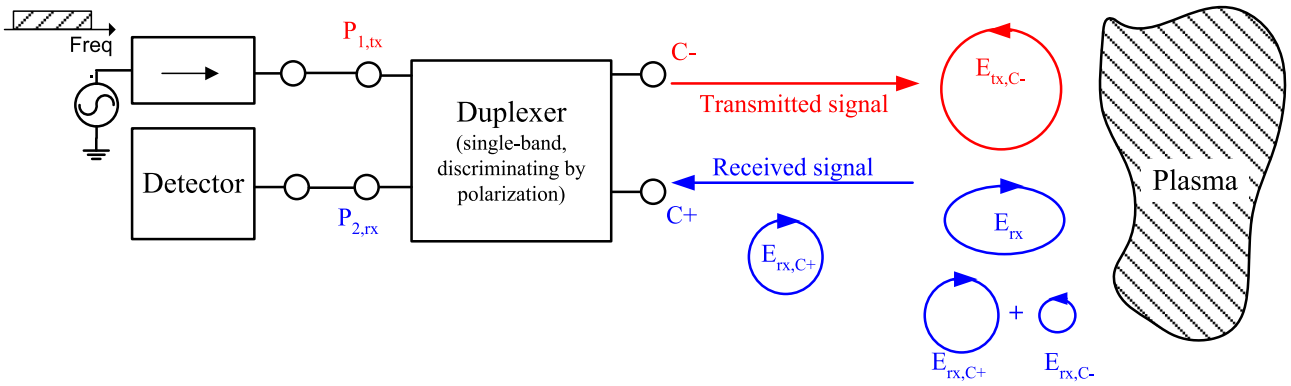

Fig. 1. Operation scheme for a duplexing based on circular polarization. A circular polarization C−is transmitted and upon the reflection, its orthogonal, *i.e.*, the C+ circular polarization is received for detection.

mechanical arrangement [19–21]. These features are crucial in plasma heating and fusion energy, albeit for high frequencies as the W-band used in this paper and above, the development of the system architecture for diverse instruments and the circuitry is still active [22–25]. The aim of this work is to develop a fully waveguide duplexer with a single horn and a single band operating at 94 GHz for use in plasma diagnosis. Moreover, the design is focused on achieving a high isolation as well as low axial ratio with the goal in mind of a large discrimination between received and transmitted signals. The approach is based on using a septum-orthomode device (septum-OMT from now on) that feeds a single circular horn antenna, optimizing their integration for obtaining a great performance, not reported so far, to the authors' knowledge, at W-band.

2. Waveguide duplexer design

The waveguide duplexer in Fig. 1 is composed of a septum-OMT and a horn antenna. Next, the detailed design of every component is described.

2.1. Septum- OMT design

A septum-OMT polarizer is a well-known passive device implemented in waveguide technology with three physical ports; two rectangular input waveguides and a square or circular output waveguide. Since it is a reciprocal device, the roles of the input and output ports are interchangeable. Because two degenerate modes can propagate in the square/circular waveguide, from an electrical point of view the septum-OMT is a four-port device. These degenerate modes are the TE_{10} and TE_{01} in the case of square waveguide and the TE_{11c} and TE_{11s} in the case of circular waveguide. The principle of operation and the detailed analysis can be found in several works, as for instance [8,26–28]. For the duplexer, the key point is that the ideal scattering matrix that characterizes the device is the following:

$$S = \frac{1}{\sqrt{2}} \begin{pmatrix} 0 & 0 & 1 & -j \\ 0 & 0 & -j & 1 \\ 1 & -j & 0 & 0 \\ -j & 1 & 0 & 0 \end{pmatrix} \tag{1}$$

A schematic of the septum-OMT polarizer including the port numbers is shown in Fig. 2. The two rectangular waveguides are connected at a junction containing a stepped septum leading to several waveguide sections of a ridge waveguide. The square waveguide is directly connected to the circular horn drastically simplifying the manufacture and reducing the cost. The stepped septum symmetrically positioned allows the efficient excitation from the rectangular waveguides of two linear and orthogonal polarizations with same amplitude and ±90 degrees phase-shifted. Finally, the superposition of the above linear polarizations leads to a circular polarized electromagnetic field.

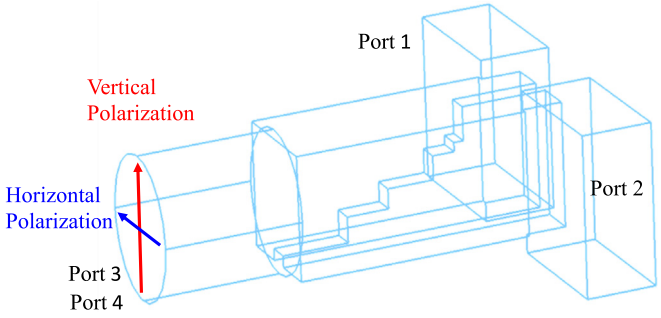

Fig. 2. (a) Geometry of the septum-OMT including the port numbers and the two modes representing the linear polarizations at the common port, vertical and horizontal, with ±90 degrees phase-shifted.

The electrical parameters to consider in its design are: the return loss ($S_{11} = S22$ by symmetry in terms of scattering parameters), the isolation (S_{21}) and the axial ratio (2), (3) between the left hand circular polarization (C−or LHCP) and the right hand circular polarization (C+ or RHCP).

The design process starts setting the thickness of the septum to assure its feasibility when manufacturing is carried out. It is an essential point since the above parameter is key to fulfill the required return loss level. Therefore, a trade-off is compulsory to obtain the matching level and the necessary stiffness from the mechanical point of view. Taking into account the operation at W-band, and the above reason, the thickness is initially fixed to 0.4 mm. Next, the number of steps in the septum, their initial length and height are chosen as seed values to the optimization process, as it is usually done in computer aided design tools [28,29]. When a single cost function is used (alternative schemes with multi-objective schemes could be used [30]), it must include the return loss (*RL*), the isolation (*IL*) and the desired axial ratio (*AR*).

The axial ratio in the actual septum-OMT is computed from the transmission to the degenerated modes with linear polarization at the common port ports, using the magnitude and phase

$$k = \sqrt{1 - \frac{4\sin 2(\theta)\,|s_{31}|^2\,|s_{41}|^2}{\left(|s_{31}|^2 + |s_{41}|^2\right)^2}} \quad \theta = \arg\left(s_{31}\right) - \arg\left(s_{41}\right), \tag{2}$$

to provide the axial ratio as:

$$ar = \sqrt{\frac{1+k}{1-k}} \tag{3}$$

The cost function (CF), depending on the physical parameters of the septum-OMT grouped in a vector **x**, is then computed as the weighted

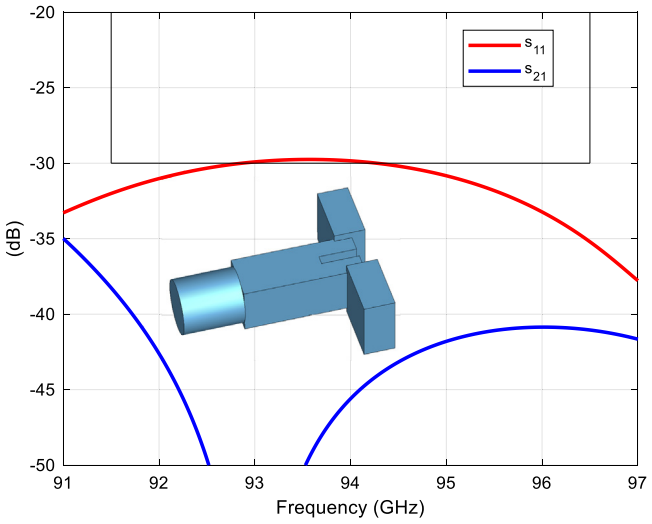

Fig. 3. Simulated response of the return loss higher than 30 dB and the isolation higher than 40 dB in the operation band 91.5–96.5 GHz. In the inset, a 3D view of the septum-OMT is shown.

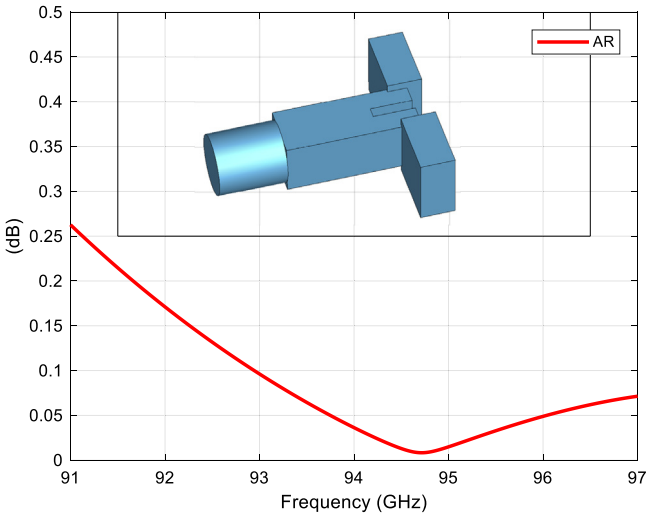

Fig. 4. Simulated response of the axial ratio, lower than 0.25 dB in the operation band (91.5–96.5 GHz). In the inset, a 3D view of the septum-OMT is shown.

sum of M frequency points in the desired bandwidth:

$$CF(\mathbf{x}) = P_1 \sum_{k=1}^{M} U\left(RL_{goal}(dB), 20\log 10\left(\frac{1}{|S_{11}|}\right)\right) + P_2 \sum_{k=1}^{M} U\left(IL_{goal}(dB), 20\log 10\frac{1}{|S_{21}|}\right) + P_3 \sum_{k=1}^{M} U\left(20\log 10ar, AR_{goal}(dB)\right) \quad (4)$$

where the S-parameters and the axial ratio depend on the actual geometry ($\mathbf{x}$), and the function $U(a, b)$ takes into account that once the goal has been obtained, its contribution to the cost function is stopped:

$$U(a,b) = \begin{cases} (|a| - |b|)^2, & |a| > |b| \\ 0, & |a| \le |b| \end{cases} \quad (5)$$

The three different weights $P_j (j = 1, 2, 3)$ in (4) are used to compensate the different level in each specification. The circular waveguide radius is included also in the optimization as a parameter inside $\boldsymbol{x}$. The specified values for the design are: $RL_{goal} \geq 30$ dB, $IL_{goal} \geq 40$ dB and the $AR_{goal} \leq 0.25$ dB. The number of steps in the septum is 5. Fig. 3 shows the simulated response using CST [31] for the return loss and the isolation in the operation band 91.5 to 96.5 GHz. This large theoretical values are necessary because the expected manufacturing accuracy is ±0.02 mm. Fig. 4 shows the axial ratio, lower than 0.25 dB.

2.2. Horn design

The design of the circular horn keeps in mind two main goals: the reflection coefficient and the radiation pattern. A dual-mode, smooth-walled profile has been chosen for ease of fabrication and low-cost compared to the corrugated option. An optimized smooth-walled profile horn has been used to obtain a far field radiation pattern with several advantages such as a symmetric radiation pattern, and a low level of cross polarization. The input radius of the circular horn is that calculated in the design of the septum-OMT described in the previous subsection. The desired specifications are a directivity greater than 21 dB, a symmetric radiation pattern at least for azimuth angles between −20° and 20°, and a minimum level of 32 dB return loss over the bandwidth 90–98 GHz.

Fig. 5 shows the simulated response of the return loss level, which is higher than 37 dB in the operation bandwidth. This value allows us to say that the duplexer return loss is mainly that obtained in the septum-OMT design. The simulated normalized radiation pattern for linear polarization at 94 GHz is shown in Fig. 6.

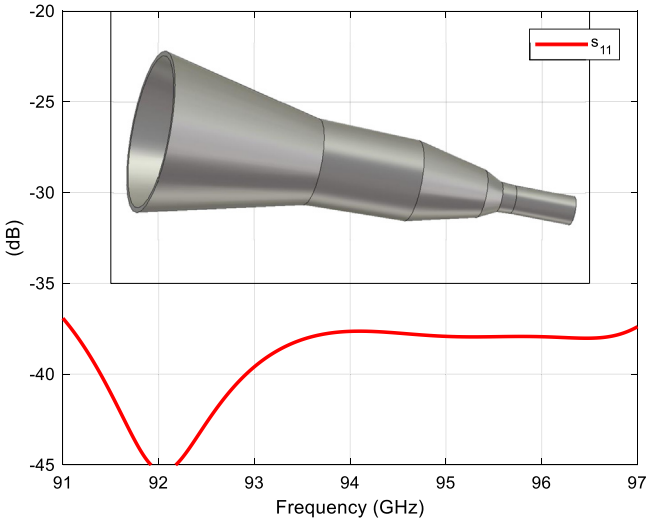

Fig. 5. Simulated return loss level higher than 37 dB in the operation band (91.5–96.5 GHz). In the inset, a 3D CAD of the antenna horn is shown.

2.3. Duplexer design

Once both devices forming the waveguide duplexer have been designed separately, they are connected through their circular ports with the same radius. Since the return loss level of the horn is 37 dB higher than the septum-OMT the only detail to consider is the connection length. The axial ratio and the isolation remain unchanged. In short, they can be designed independently.

3. Mechanical design and fabrication

As previously stated, since the beginning of the design process a close relationship with the mechanical team has been maintain to carry our successfully the manufacture. The septum-OMT has been divided into two brass blocks, corresponding to the body and the cover, as it can be observed in Fig. 7a. In order to be confident with the contact

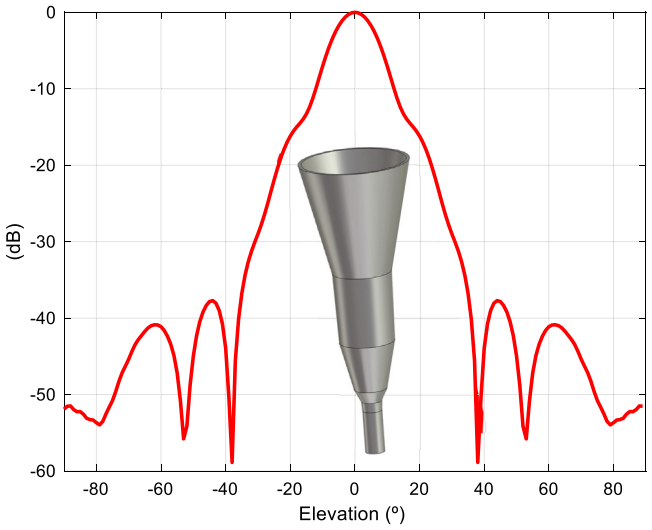

Fig. 6. Simulated normalized radiation pattern of the designed horn for linear polarization at 94 GHz. In the inset, a 3D CAD of the antenna horn is shown.

between both pieces, a crucial point to control the losses, a part of the rectangular output waveguides has been electro-eroded in the cover for the purpose of ensuring flatness. Besides, the accuracy in the alignment between them is 0.01 mm. The conical horn antenna is a single brass block carefully aligned to the septum-OMT and fixed by means of two pins to assure the axial ratio, avoiding possible degradation of the cross polar level caused by misalignment errors, as discussed in [3] and [4].

In both manufacturing processes, *i.e.*, Electrical Discharge Machining (EDM) for the horn antenna and Computer Numerical Control (CNC) milling for the septum-OMT, the tolerance has been ±0.02 mm. Fig. 7b shows the manufactured waveguide duplexer.

4. Experimental results

The duplexer has been experimentally characterized measuring its scattering parameters by means of the Vectorial Network Analyser (VNA) and the radiation pattern in the anechoic chamber. Fig. 8a shows the duplexer connected to the extended ports of the VNA at the W-band. A TRL calibration in WR10 waveguide standard has been carried out to measure the return loss and the isolation between input ports. In Fig. 8b the device positioned in the anechoic chamber to measure the radiation pattern is shown.

In Fig. 9 the comparison between the simulation and the measurement of the return loss level is shown for both polarizations under excitation by ports P_1 and P_2 (3D CAD of the inset of Fig. 9). As can be observed, this level is higher than 30 dB in the complete operation band (5 GHz). In addition the two measurement are quite similar, showing an excellent manufacturing process. Fig. 10 shows the comparison between the simulation and the measurement of the isolation between ports P_1 and P_2 of the duplexer, with a measured value better than 30 dB. Fig. 11 shows the measured results for the axial ratio, exciting by the rectangular ports P_1 and P_2. They are very similar, which implies that the manufacture has been very accurate, maintaining the axial symmetry. The discrepancy between the simulation and the two experimental results is explained considering the manufacturing tolerance of ±0.02 mm. The sensitivity of the axial ratio with respect to small deviations in the manufacturing is a well-known feature of septum-OMTs [26–28], since this parameter involves not only amplitudes, but

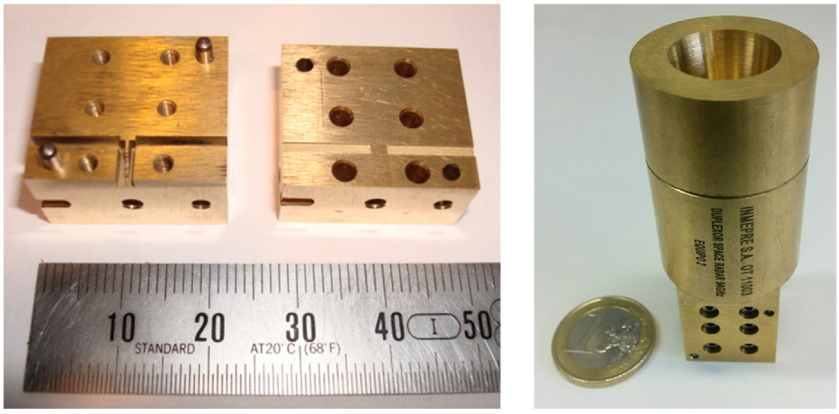

(a) (b)

Fig. 7. (a) Two brass blocks (body and cover) of the septum-OMT manufactured by electrical discharge machining (EDM). (b) Manufactured waveguide duplexer composed of the septum- OMT and the conical horn.

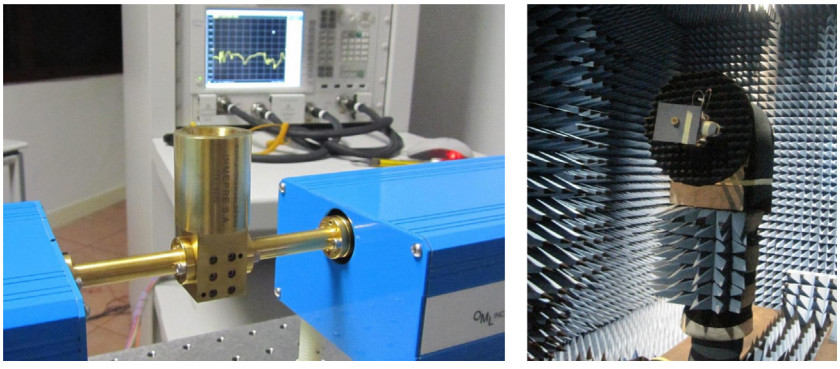

Fig. 8. (a) Workbench for the scattering parameter measured using the VNA. (b) Duplexer positioned in the anechoic chamber to measure the radiation pattern.

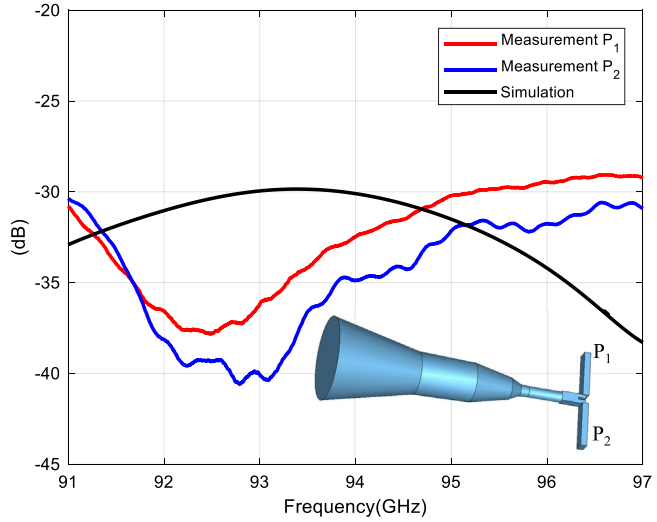

Fig. 9. Comparison between the simulation and the measurement of the return loss level of the duplexer in ports P_1 and P_2. In the inset a 3D CAD view of the diplexer is shown.

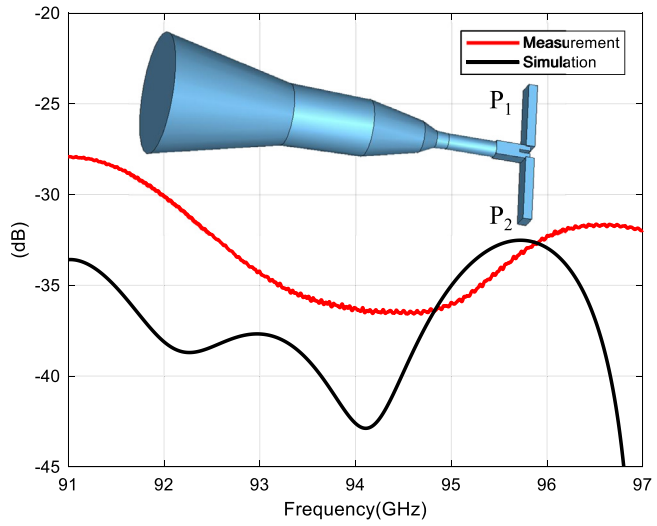

Fig. 10. Comparison between the simulation and the measurement of the isolation between ports P_1 and P_2 of the duplexer. In the inset a 3D CAD view of the diplexer is shown.

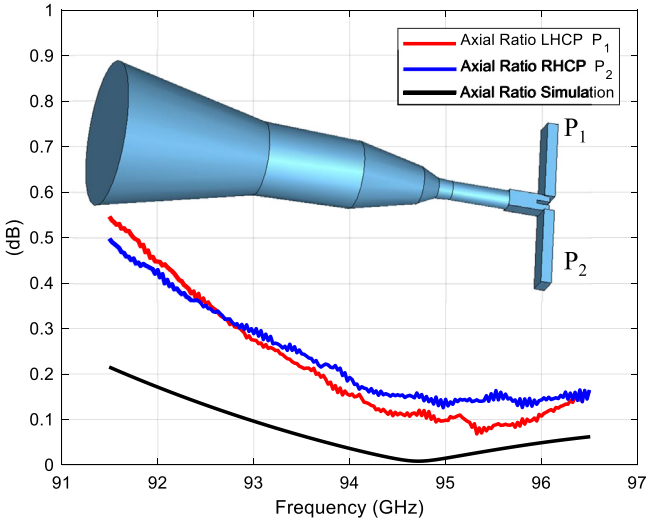

Fig. 11. Comparison between the simulation and the measurement of the axial ratio for both circular polarizations. In the inset a 3D CAD view of the diplexer is shown.

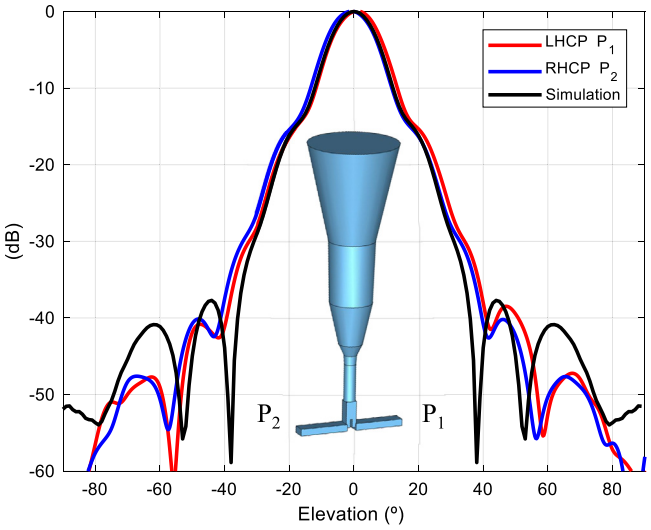

Fig. 12. Comparison between the simulation and the measurement of the normalized co-polar radiation pattern (Phi = 0) of both circular polarizations at 94 GHz. In the inset a 3D CAD view of the diplexer is shown.

also phases of the orthogonal field components. In this case, taking into account the high operation frequency of the design (W band), the experimental result can be considered excellent.

The response in radiation is shown in Figs. 12 and 13. Fig. 12 shows the measured normalized radiation pattern of both circular polarizations, which are very close to the simulated performance. Finally, the full co-polar and cross-polar radiation pattern for the LHCP and RHCP are shown in Figs. 13 and 14 respectively.

5. Conclusion

In this work, the design and characterization of a waveguide duplexer at 94 GHz for plasma diagnosis has been presented. The duplexing process is based on transmitting and receiving orthogonal circular polarizations by means of a septum-OMT and a single horn antenna. This configuration leads to the most simple and compact option for a single-band operation. A systematic process has been followed designing both components, *i.e.*, the septum OMT and the circular horn to obtain their dimensions. In the case of the horn, only one quarter of the structure has been considered in the design taking into account its two symmetry planes. As a results, the computational effort has been dramatically reduced. The manufacturing process by means of high precision micromachining has led to the excellent measured performance, especially the axial ratio, a key parameter to discriminate between polarizations.

Acknowledgment

The authors would like to thank to INMEPRE S.A., the diligence in the manufacturing process. This work was supported by the Spanish government under grants (ADDMATE) TEC2016-76070-C3-1/2-R (Agencia Estatal de Investigación, Spain, Fondo Europeo de Desarrollo Regional: AEI/FEDER/UE) and the program of Comunidad de Madrid, Spain S2013/ICE-3000 (SPADERADARCM).

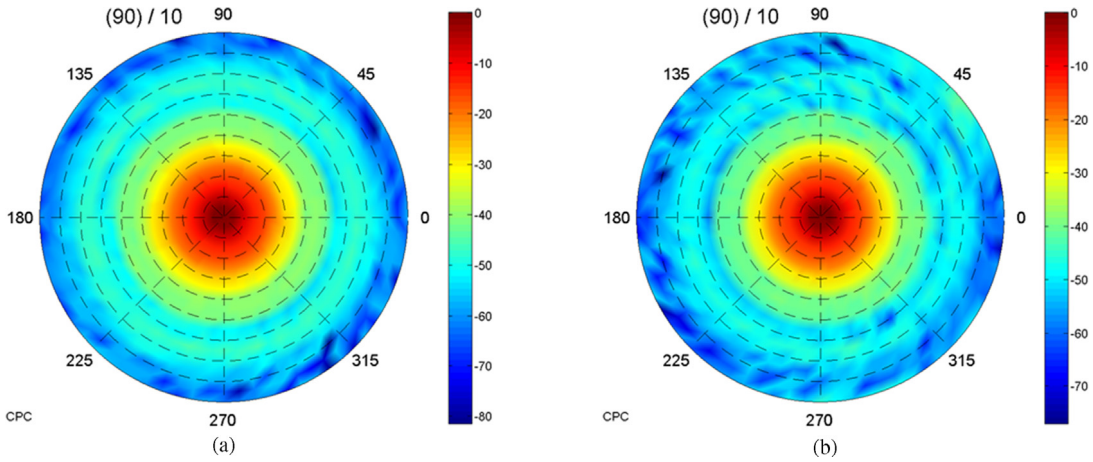

Fig. 13. (a) Measured normalized full co-polar radiation pattern for the LHCP at 94 GHz. (b) Measured normalized full co-polar radiation pattern for the RHCP at 94 GHz.

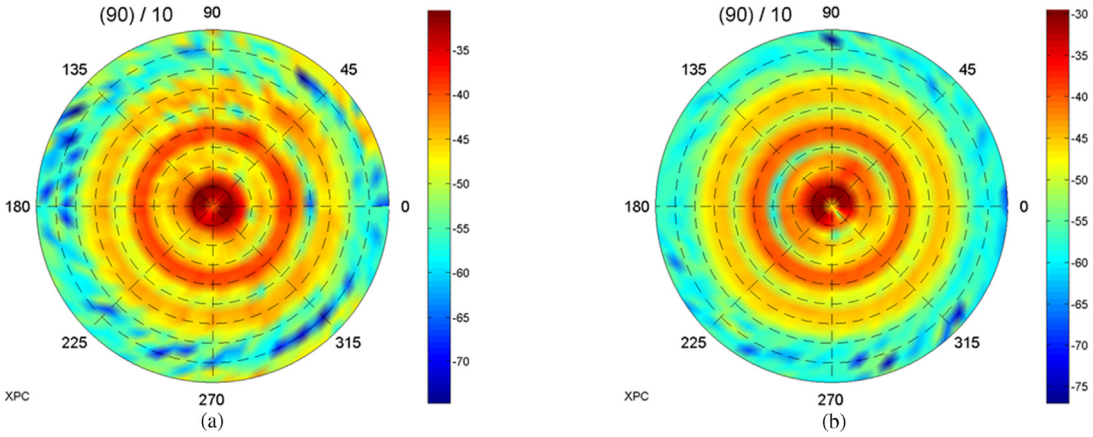

Fig. 14. (a) Measured normalized full cross-polar radiation pattern for the LHCP at 94 GHz. (b) Measured normalized full cross-polar radiation pattern for the RHCP at 94 GHz.

References

[1] S.K. Rao, Advanced antenna technologies for satellite communications payloads, IEEE Trans. Antennas Propag. 63 (4) (2015) 1205–1217.

[2] S. Rao, J. Kralovec, Compact high-performance reflector-antenna feeds and feed networks for space applications [antenna applications], IEEE Antennas Propag. Mag. 52 (4) (2010) 210–217.

[3] A. Dunning, S. Srikanth, A.R. Kerr, A simple orthomode transducer for centimeter to submillimeter wavelengths, in: Proc. 20th Int. Symp. on Space THz Technol, Charlottesville, VA, USA, 1990.

[4] C. Groppi, A. Navarrini, G. Chattopadhyay, A waveguide orthomode transducer for 385–500 GHz, in: Proc. 18th Int. Symp. on Space THz Technol., 2010, pp. 23–25.

[5] G.M. Coutts, Octave bandwidth orthomode transducers for the expanded very large array, IEEE Trans. Antennas Propag. 59 (6) (2011) 1910–1917.

[6] K.B. Cooper, R. Dengler, N. Llombart, B. Thomas, G. Chattopadhyay, P. Siegel, THz imaging radar for standoff personnel screening, IEEE Trans. Terahertz Sci. Technol. 1 (1) (2011) 169–182.

[7] K.B. Cooper, G. Chattopadhyay, Submillimeter-wave radar: Solid-state system design and applications, IEEE Microw. Mag. 15 (7) (2014) 51–67.

[8] C.A. Leal-Sevillano, K.B. Cooper, J.A. Ruiz-Cruz, J.R. Montejo-Garai, J.M. Rebollar, A 225 GHz circular polarization waveguide duplexer based on a septum orthomode transducer polarizer, IEEE Trans. Terahertz Sci. Technol. 3 (5) (2013) 574–583.

[9] J.A. Ruiz-Cruz, J.R. Montejo-Garai, J.M. Rebollar, Optimal configurations for integrated antenna feeders with linear dual polarization and multiple frequency bands, IET Microw. Antennas Propag. 5 (8) (2011) 1016–1022.

[10] H. Siegel, Terahertz technology, IEEE Trans. Microw. Theory Tech. 50 (3) (2002) 910–928.

[11] B.J. Drouin, F.W. Maiwald, J.C. Pearson, Application of cascaded frequency multiplication to molecular spectroscopy, Rev. Sci. Instrum. 76 (9) (2015) 093113–1–093113–10.

[12] N.C. Luhmann, W.A. Peebles, Instrumentation for magnetically confined fusion plasma diagnostics, Rev. Sci. Instrum. 55 (3) (1984) 279–331.

[13] J.R. Montejo-Garai, C.A. Leal-Sevillano, J.A. Ruiz-Cruz, J.M. Rebollar, T. Estrada, Synthesis and design of waveguide band-stop filters without out-of-band spurious responses for plasma diagnosis, Fusion Eng. Des. 89 (9) (2012) 1662–1666.

[14] M.P. Bachynski, B.W. Gibbs, K.A. Graf, Reflection of circularly polarized electromagnetic waves from an anisotropic plasma, Radio Sci. 2 (8) (1967) 881–892, http://dx.doi.org/10.1002/rds196728881.

[15] S.E. Segre, V. Zanza, Polarization of radiation in incoherent Thomson scattering by high temperature plasma, Phys. Plasmas 7 (6) (2000) 2677–2684, http://dx.doi.org/10.1063/1.874110.

[16] E. Parke, V.V. Mirnov, D.J. Den Hartog, A polarization-based Thomson scattering technique for burning plasmas, J. Instrum. 9 (2) (2014) C02030.

[17] V.V. Mirnov, D.J. Den Hartog, E. Parke, Exact relativistic expressions for polarization of incoherent Thomson scattering, Phys. Plasmas 23 (5) (2016) 052108, http://dx.doi.org/10.1063/1.4948488.

[18] Z.M. Ng, L.E. Davis, R. Sloan, Measurements of V-band n-type InSb junction circulators, IEEE Trans. Microw. Theory Tech. 52 (2) (2004) 482–488.

[19] R. Kumar, M. Jose, G.N. Singh, G. Kumar, P.V. Bhagwat, RF characterization and testing of ridge waveguide transitions for RF power couplers, Nucl. Instrum. Methods Phys. Res. A 838 (2016) 66–73.

[20] J. Liu, J. Shi, J. Qiu, H. Chen, X. Wu, Development of a high-power X-band compact RF rotary joint, Nucl. Instrum. Methods Phys. Res. A 908 (2018) 72–77.

[21] X. Meng, J. Shi, H. Zha, Q. Gao, Z. Liu, J. Liu, J. Qiu, Development of high-power S-band load, Nucl. Instrum. Methods Phys. Res. A 927 (2019) 209–213.

[22] T.R. Stevenson, W.T. Hsieh, G. Schneider, D. Travers, N. Cao, E. Wollack, M. Limon, A. Kogut, Building blocks for a polarimeter-on-a-chip, Nucl. Instrum. Methods Phys. Res. A 559 (2) (2006) 611–613.

[23] S. Ali, S. Malu, D. McCammon, K.L. Nelms, R. Pathak, P.T. Timbie, D.W. van der Weide, Antenna-coupled transition-edge hot-electron microbolometer, Nucl. Instrum. Methods Phys. Res. A 520 (1–3) (2004) 490–492.

[24] F. Cuttaia, L. Valenziano, M. Bersanelli, R.C.D. Butler, O. D'Arcangelo, D. Kettle, G. Morigi, Analysis of the radiometer—reference load system on board the Planck/LFI instrument, Nucl. Instrum. Methods Phys. Res. A 520 (1–3) (2004) 396–401.

[25] J.R. Montejo-Garai, J.A. Ruiz-Cruz, J.M. Rebollar, 5-way radial power combiner at W-band by stacked waveguide micromachining, Nucl. Instrum. Methods Phys. Res. A 905 (11) (2018) 91–95.
[26] J. Uher, J. Bornemann, U. Rosenberg, Waveguide Components for Antenna FeedSystems, Artech House, Boston, 1993.
[27] J. Esteban, J.M. Rebollar, Field theory CAD of septum OMT polarizers, in: Antennas Propag. Society International Symposium, 1992. AP-S, vol. 4, Jul. 1992, pp. 2146–2149.
[28] J. Bornemann, V.A. Labay, Ridge waveguide polarizer with finite and stepped-thickness septum, IEEE Trans. Microw. Theory Tech. 43 (8) (1995) 1782–1787.
[29] T. Itoh (Ed.), Numerical Techniques for Microwave and Millimeter-Wave Passive-Structures, John Wiley, New York, 1989.
[30] M. Kranjčević, A. Adelmann, P. Arbenz, A. Citterio, L. Stingelin, Multi-objective shape optimization of radio frequency cavities using an evolutionary algorithm, Nucl. Instrum. Methods Phys. Res. A 920 (2019) 106–114.
[31] CST, Computer simulation technology, https://www.cst.com/.